Non-Intrusive Measurement Setup for Time-Variant Mains Impedances Within the 16 kHz - 256 kHz Band

Maarten Appelman[1], Niek Moonen[1], Frank Leferink[1,2]
[1]University of Twente, Enschede, the Netherlands
[2]THALES Nederland B.V., Hengelo, the Netherlands
m.b.appelman@student.utwente.nl

***Abstract*—A non-intrusive network impedance measurement setup, aimed at live mains networks, is proposed. The system is able to measure in both time- and frequency domain, and links the measured impedance to the phase of the mains voltage signal. The method is based on the transmission parameters of the injecting and receiving probes. This paper covers the theory behind transmission parameters, a characterization method for current transformers, the measurement setup- and algorithm, and a discussion of its results by means of analysis and recommendations.**

***Index Terms*—Time-variant mains impedance, transmission parameters, current transformer characterization, non-intrusive.**

I. Introduction

The mains impedance is an essential parameter for predicting the emission levels generated by its loads. Methods for measuring this mains impedance have been around for quite some time [1] [2]. Most of them however, assume the impedance to be stable over the full 50 Hz voltage cycle. International EMC-standards such as the CISPR 22 [3] also seem to imply the mains impedance to be relatively stable, it suggests the impedance to be varying over frequency, not time. The increasing number of 'dirty' loads make these ideas sound myopic. Fig. 1 visually shows that LED-lamps often have a non-continuous power consumption, as they rapidly switch between an on- and off-state. Most modern equipment use similar techniques in order to decrease their power consumption. While the mains voltage is virtually time-invariant in terms of shape, frequency, and amplitude, the current dissipation of these mains' loads is not. If the dissipated power and current are not constant in time, it follows logically that the impedance is neither.

As mains connected electronic equipment, and technology in general, is continuously evolving and becoming increasingly sophisticated, so is their demand for electromagnetic immunity i.e. their need for good mains filtering. Having knowledge about the mains impedance should be of interest for powerline communication engineers as well, for this information can be valuable in simultaneously reducing their emitted interference and increasing their throughput [4]. Furthermore, research conducted at the University of Twente showed that measurement errors from static energy meters are highly correlated to the grid impedance [5].

Fig. 1: Photographing LED-lamps with a moving camera at a high shutter speed reveals their non-continuous power consumption

Measurement systems such as [6], [7] and [8] only measure the network impedance in the frequency domain. Which has become insufficient for a proper mains impedance measurement, given the non-continuous power consumption of modern electronic equipment. Other setups, [1] for instance, are able to measure a network impedance in the time-domain, but rely in an FFT algorithm to translate the measurement into the frequency domain. Therewith ignoring potential frequency dependent impedances. While the setup described in [9] accurately measures in both aforementioned domains, it is based on an intrusive method which encompasses significantly more expensive equipment and a large external setup.

A novel measurement setup is hence proposed for time-variant mains impedances based on the non-intrusive impedance monitoring setup described in [10]. The setup in [10] differs from the proposed system as this paper also encompasses measurements in the frequency domain, and is focused on a network with a high local AC voltage. Key issues in both the characterization of the probes and the measurement method that were either not encountered or mentioned in [10] will here be elaborated on as well. While the suggested measurement method is also applicable to other networks, it involves a few elements specifically implemented for mains impedance measurements.

This paper adheres to the following outline: section II describes the theory behind the transmission parameters, and the characterization process of the mains network and the current transformers. Section III explains the proposed measurement setup and its requisite apparatus, while section IV clarifies the suggested measurement algorithm. The measurement results are discussed in section V. Finally, section VI gives a conclusion to the complete research and section VII gives recommendations in order to improve the proposed measurement setup.

II. Theory

A. The transmission matrix

Given the objective of the proposed measurement setup (finding the time-variant mains impedance) using either impedance- or admittance parameters would seem like the most straightforward approach in completing it. Given however, that non-intrusive current injection has a very inductive character, Z- and Y-matrices become quite problematic. When injecting a signal with an inductive clamp and receiving that signal with a second inductive clamp a two-port network is created where the clamp's impedances make the mains impedance negligibly low.

The transmission matrix, also known as the ABCD-matrix, allows to avoid this problem by separating the parameters of the probes from those of the grid. The transmission matrix is in its very essence a tool to solve the equations from (1). It provides a means to calculate both the voltage and current at one port of a two-port network with the voltage and current at the other port.

$$V_1 = AV_2 + BI_2 \tag{1a}$$

$$I_1 = CV_2 + DI_2 \tag{1b}$$

The transmission parameters are defined by (2), where port 2 is either cut short or left as an open port. It should be noted that this definition uses the newest convention from [11], where the input current has the same direction as the output current. This form makes it less complicated to describe a series of two-port networks. In fact, when (1) is put in a matrix form, it can be seen that a series of two-port networks can be described by the cross-product of their respective transmission matrices multiplied by their output voltage.

$$A = \left.\frac{V_1}{V_2}\right|_{I_2=0} \quad \text{(2a)} \qquad B = \left.\frac{V_1}{I_2}\right|_{V_2=0} \quad \text{(2b)}$$

$$C = \left.\frac{I_1}{V_2}\right|_{I_2=0} \quad \text{(2c)} \qquad D = \left.\frac{I_1}{I_2}\right|_{V_2=0} \quad \text{(2d)}$$

This can be illustrated by considering Fig. 2 and (1), which allows to construct the following equation:

$$\begin{bmatrix} V_2 \\ I_2 \end{bmatrix} = \begin{bmatrix} A_2 & B_2 \\ C_2 & D_2 \end{bmatrix} \times \begin{bmatrix} V_3 \\ I_3 \end{bmatrix} \tag{3}$$

Hence, the input parameters can be found by:

$$\begin{bmatrix} V_1 \\ I_1 \end{bmatrix} = \begin{bmatrix} A_1 & B_1 \\ C_1 & D_1 \end{bmatrix} \times \begin{bmatrix} A_2 & B_2 \\ C_2 & D_2 \end{bmatrix} \times \begin{bmatrix} V_3 \\ I_3 \end{bmatrix} \tag{4}$$

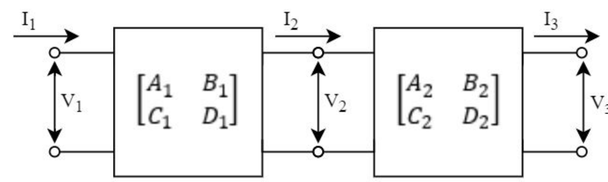

Fig. 2: A series of two-port networks

It follows that this method, of evaluating a cascade of two-port networks by taking the cross product of their respective transmission matrices, can be extended ad infinitum.

B. Building transmission matrices

The proposed measurement setup relies on an injection probe inducing a current in the Network Under Test (NUT) and a receiving probe to determine how the NUT transformed the injected signal. By placing these probes at the output of a wall socket, the circuit shown in Fig. 4 is created. In pursuance to the method described in [10] the received signal will be assessed on both the in- and output parameters of the cascaded two-port networks as on the transmission parameters of these networks.

1) Characterizing mains network: Using standard network theory, the NUT in Fig. 4 can be reduced to the two-port network shown in Fig. 3. Where the input port corresponds to the position of the injecting probe, the output to the receiving probe, and Z to the cumulative impedance of all devices and wires attributing to the impedance found between port 1 and 2.

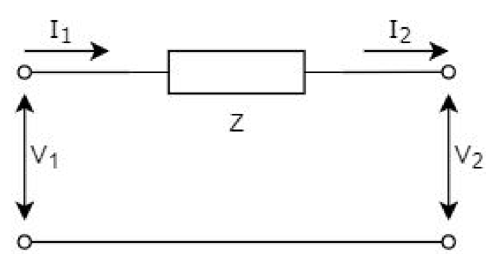

Fig. 3: NUT reduced to a two-port network

Applying (2) to the circuit shown in Fig. 3 yields the transmission matrix shown in (5). This matrix now only

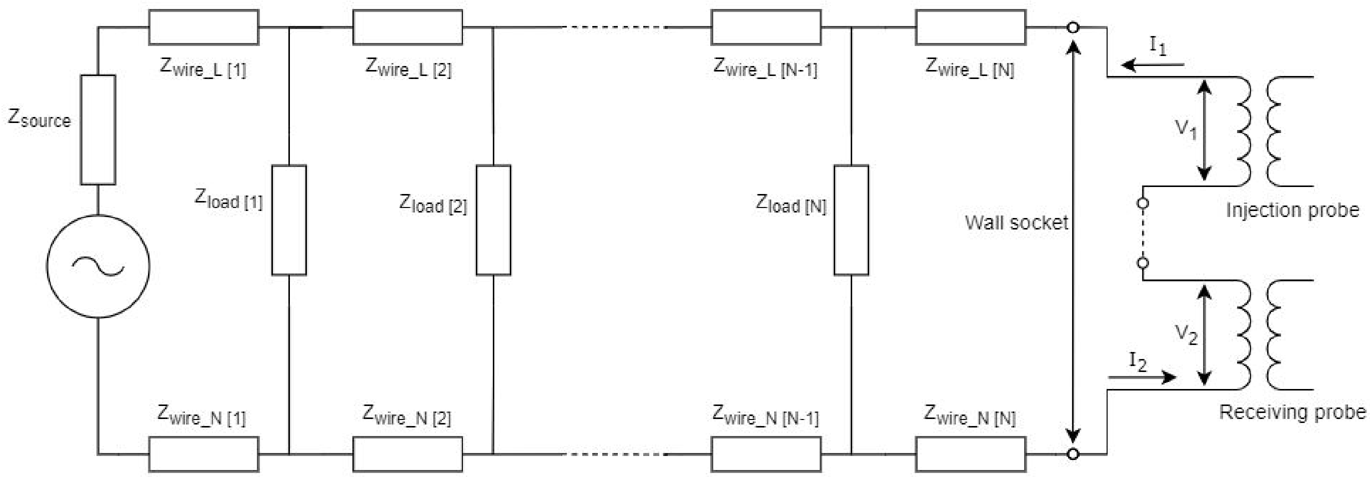

Fig. 4: Injection- and receiving probe connected to mains

holds one variable, which fortunately happens to be the mains impedance itself.

$$\begin{bmatrix} A_{Mains} & B_{Mains} \\ C_{Mains} & D_{Mains} \end{bmatrix} = \begin{bmatrix} 1 & V/I \\ 0 & 1 \end{bmatrix} = \begin{bmatrix} 1 & Z \\ 0 & 1 \end{bmatrix} \quad (5)$$

2) Characterizing current transformers: Assuming the characteristics of the current transformers to be constant over time, and independent of its input voltage- and current, they can be characterized using the method described in [6]. While [6] sufficiently describes the used characterization method, it is still beneficial to describe it here as it has significant implications for the proposed measurement setup.

The transmission matrix of a two-port network can be retrieved from the combination of its scattering parameters, and the input impedance (Z_0) of the analysis equipment used to measure them [11]. The current transformers can therefore be characterized using only a calibration fixture and a VNA. The characterization setup for the injection probe is shown in Fig. 5, where port 1 of the VNA is connected to the probe, and port 2 is connected to the fixture. The fixture is terminated by a 50 Ω impedance ($Z_{fixture}$), and the receiving probe is connected to a high pass filter (to filter out the 50 Hz mains signal) which is then terminated by a 50 Ω impedance (Z_{rec}) to account for parasitic behavior such as resonances. Characterizing the receiving probe is similar, the injection probe must be terminated by a 0 Ω impedance (Z_{inj}) to mimic the amplifier's low ohmic output impedance, the high pass filter should be placed between the receiving probe and port 2, and either the obtained S-parameters or the connections to port 1 and 2 should be reversed.

It should be noted that this method will not only characterize the probes, but the 50 Ω load impedance ($Z_{fixture}$) as well. Since the measurement setup is modeled as a series of three two-port networks, these loads can be translated to the mains

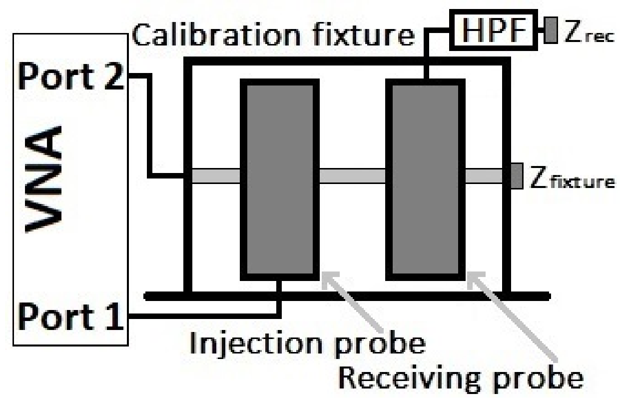

Fig. 5: Injection probe characterization setup

transmission matrix. Utilizing this method, the B-parameter of the mains transmission matrix does not equal Z, but Z - 100 Ω.

$$\begin{bmatrix} V_1 \\ I_1 \end{bmatrix} = \begin{bmatrix} A_{Inj} & B_{Inj} \\ C_{Inj} & D_{Inj} \end{bmatrix} \times \begin{bmatrix} 1 & Z-100 \\ 0 & 1 \end{bmatrix} \times \begin{bmatrix} A_{Rec} & B_{Rec} \\ C_{Rec} & D_{Rec} \end{bmatrix} \times \begin{bmatrix} V_2 \\ I_2 \end{bmatrix} \quad (6)$$

Representing the proposed measurement setup in its ABCD-parameters (6) provides a means to find the mains impedance Z:

$$Z = \frac{V_1 - A_{inj} \cdot M - B_{inj} \cdot N}{A_{inj} \cdot N} + 100 \quad (7)$$

Where:

$$\begin{aligned} M &= V_2 \cdot A_{rec} + I_2 \cdot B_{rec} \\ N &= V_2 \cdot C_{rec} + I_2 \cdot D_{rec} \end{aligned} \quad (8)$$

III. Measurement setup

The parameters that the proposed measurement setup needs to measure are given by (7). V_1 and V_2 can be measured directly at the input of the injection probe and the output of the receiving probe, respectively. The receiving probe should be terminated by a low ohmic e.g. $50\,\Omega$ load impedance rather than the oscilloscope's $1\,\mathrm{M}\Omega$ input impedance in order for it to generate a measurable current. consequently, I_2 can be found by dividing V_2 by its load impedance. The line-neutral or line-earth voltage should be recorded as well in order to link the found impedance to the mains' phase.

The proposed measurement setup is depicted in Fig. 6. Where, in addition to the aforementioned equipment, a $100\,\Omega$ load and an amplifier are included to prevent a short at the wall socket and increase the input signal, respectively. Each element in the setup will be considered here individually.

A. Equipment

1) Data acquisition + AWG
   A PicoScope 4824 is used to acquire the three voltages displayed in Fig. 6, and to generate the system's input signal. The collected data is processed in Matlab. The AWG has a 1 MHz bandwidth, which is sufficient for the intended purpose. The scope is capable of acquiring data at a 12 bit resolution, which can be extended to 16 bits by reducing the sampling rate and oversampling the input signals.

2) Current transformers
   The receiving probe has been built by hand and was optimized empirically. It encompasses a combination of six current transformers connected in parallel. They are wound around of-the-shelf ferrite rings with a permeability determined at $\mu \approx 3740\,\mathrm{H/m}$. The injection probe is a handmade off-the-shelf current transformer with a comparable permeability. The probes where tested on a calibration fixture, terminated at $50\,\Omega$, their S_{21} parameters are displayed in Fig. 7. Both transformers are reciprocal, which make them interchangeable with respect to the measurement signal. It is however advantageous to use the transformer with the highest attenuation at 50 Hz as the receiving probe in order to suppress noise and increase the dynamic range.

3) Amplifier
   The system requires an amplifier able to operate within the range of 16 - 255 kHz. The signals below 125 kHz will be amplified by an audio amplifier (Solar Electronics, Model 6552-1A) while the signals above this frequency will be handled by an RF amplifier (Kalmus, Model 110C).

4) Load
   In order to prevent the measurement setup from creating a short between the Line and Neutral connections of the mains network, a load has to be implemented. There are multiple considerations when picking the value of this load. Imprimis, the load should exceed a certain minimal impedance in order to prevent circuit breakers from tripping, this equates to roughly $15\,\Omega$ for standard European $230\,V$ networks. Furthermore, there exists a trade-off where a high impedance reduces both the signal strength and the heat dissipation. A value of $100\,\Omega$ is chosen as an estimated equal substitution. Placing this load in series with the NUT reduces (7) to:

$$Z = \frac{V_1 - A_{inj} \cdot M - B_{inj} \cdot N}{A_{inj} \cdot N} \tag{9}$$

   The load is build out of two aluminum 200 Ω resistors, placed in parallel and complemented by a DC powered cooling block. Preventing the DC power supply from introducing noise in the system can be done by either using batteries or by implementing a galvanic isolation between the net and the AC-DC converter.

5) High-pass filter
   The local voltage signal of the NUT forms a serious noise source in this measurement setup. While digital filtering brings an advantage in adjustability, it does not account for the loss of dynamic range caused by the parasitic modulation of the injected signal by the local AC voltage. An analog filter lacks mobility but utilizes the available resolution more efficiently. A 1 kHz 5^{th} order elliptic high pass filter is used in the current setup. It provides an attenuation below -61.5 dB for the local 50 Hz mains signal and a 0 dB passband for the frequency band of interest.

6) Breakout box
   While this measurement setup can be applied to other networks, it is built specifically for single-phase mains networks. Measuring the time-variant impedance of these networks is assumed to be of equal interest as the phase-variant impedance i.e. this impedance is assumed to be cyclo-stationary with a 20 ms period (analogous to the mains voltage). The transmission parameters, therewith (9), account for the attenuation/amplification as well as the phase shifts of the two port networks. Hence, by measuring the mains voltage parallel to V_1 and V_2 the determined impedance can be paired directly to phase of the mains signal.

B. validation

Three individual setups have been built to validate (9) and the retrieved transmission parameters from section II-B2. All setups are built around a calibration fixture, and are depicted in Fig. 9. The validation of the ABCD-matrices is done by calculating V_1 from V_2 and comparing it with the measured V_1. For the setups in Fig. 9a and Fig. 9b, V_1 can be calculated

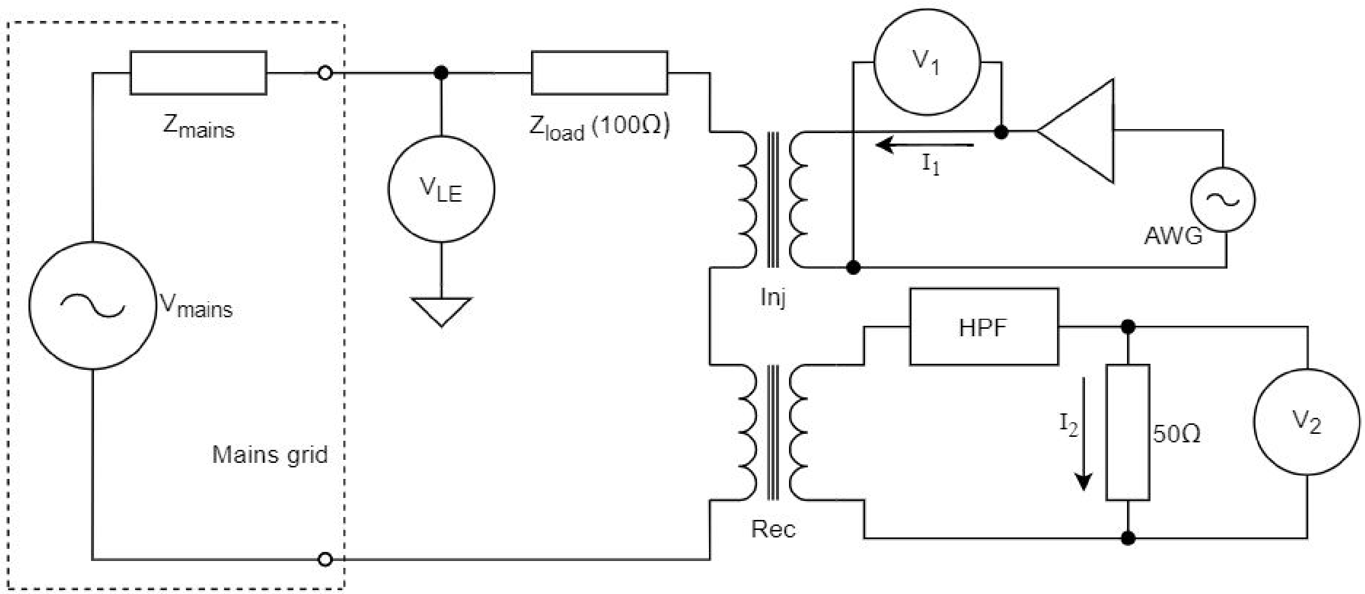

Fig. 6: Measurement setup

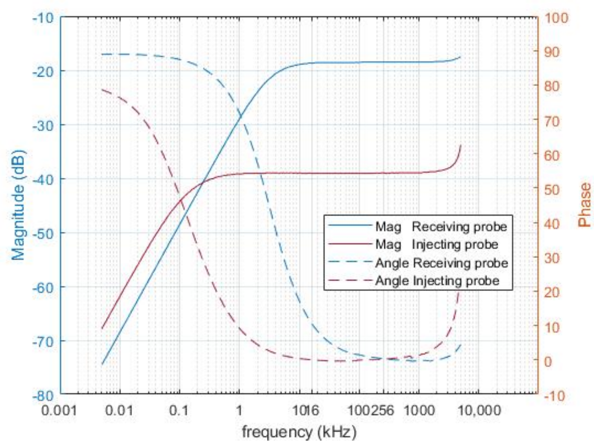

Fig. 7: Probe characterization

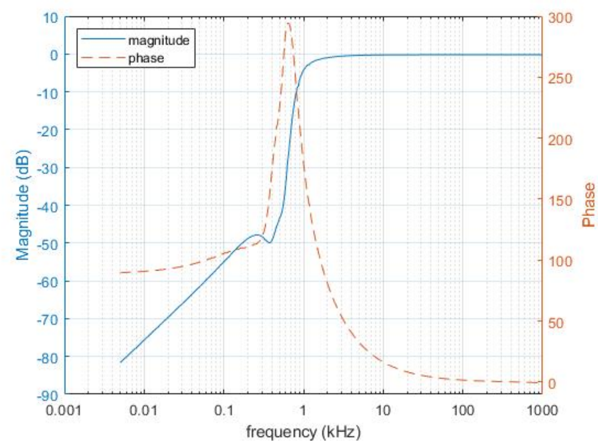

Fig. 8: HPF characterization

according to (1a), where $I_2 = \dfrac{V_2}{50}$.

In Fig. 9d and Fig. 9e a sinusoidal signal is generated, amplified and accurately retrieved by means of the determined transmission parameters, demonstrating legitimate transmission parameters, ergo a correct characterization of both probes. Fig. 9g and Fig. 9h were constructed to check for possible phase errors of (multiples of) 180 degrees, which have now been shown not to occur. The setup's ability to measure impedance in both time- and frequency domain is displayed in Fig. 9f and Fig 9i, respectively. V_1 and V_2 are included in Fig. 9f to provide a more visual explanation of [9]. Fig. 9f shows an accurate estimation of the time-varying impedance with sharp transitions between the distinct impedance levels. The frequency domain measurement (Fig. 9i) shows slight deviations in the lower frequency region, this phenomenon is further elaborated on in section V-A.

IV. Methodology

The constructed impedance equation yields the NUT's impedance in time-domain for a given frequency. This implies that information about the NUT's impedance in frequency-domain can be be retrieved by running a series of measurements at distinct frequencies. Obtaining the FFT of a single measurement would not be very insightful as this will not account for frequency dependent impedance's such as (parasitic) capacitors, chokes and filters.

The measurement algorithm is shown in Fig. 10. Where the DAQ (data acquisition) captures 40 ms seconds of data

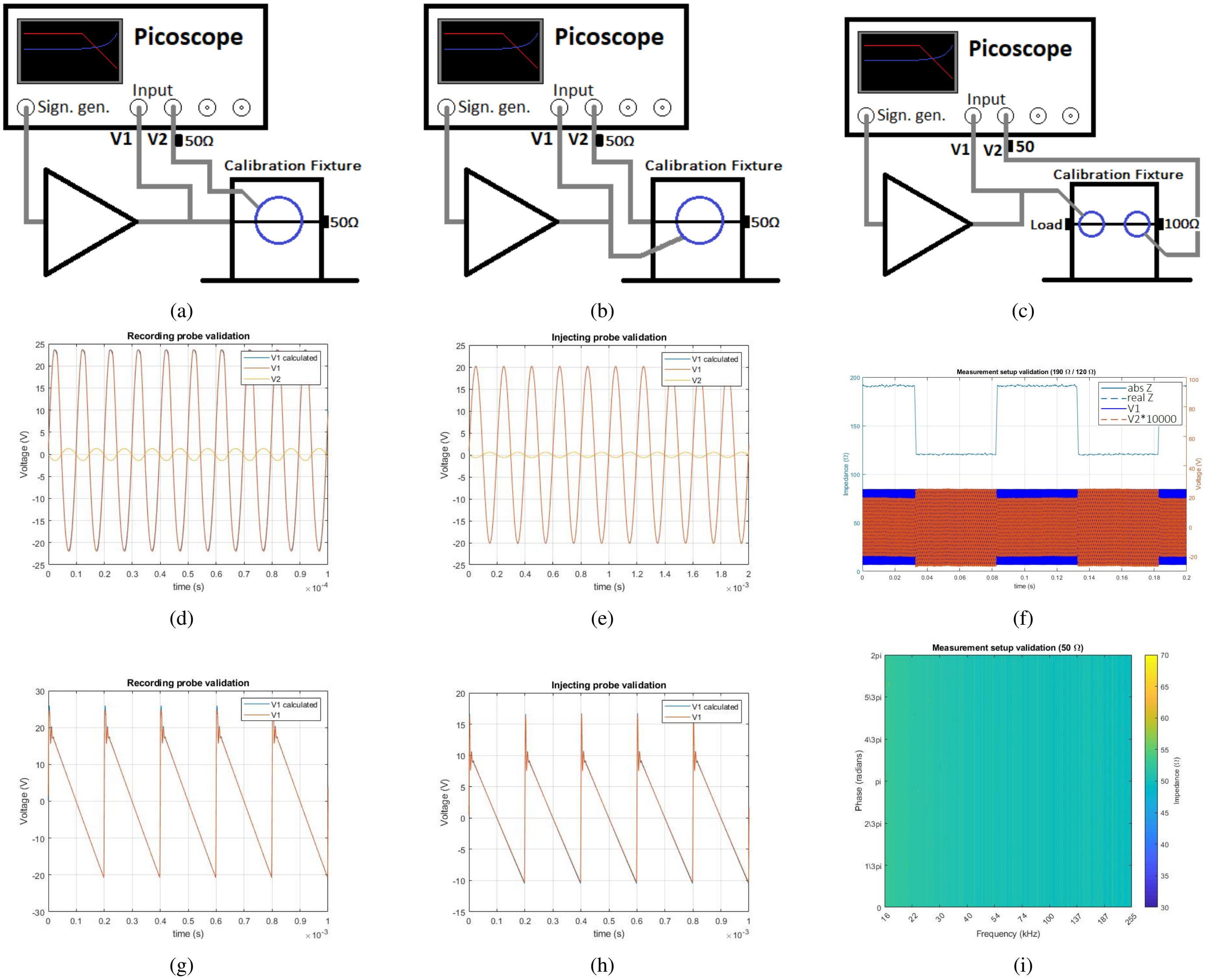

Fig. 9: Setup validation: (a) receiving probe; (b) injecting probe; (c) measurement setup; (d) receiving probe, sinusoid; (e) injecting probe, sinusoid; (f) measurement setup, time domain; (g) receiving probe, sawtooth; (h) injecting probe, sawtooth; (i) measurement setup, frequency domain

for each distinct frequency of interest. The input signals V_1 and V_2 are then (digitally) low-pass filtered to eliminate the quantization noise. If needed, other filters can be applied here as well to filter out potential residuary local signals from the NUT.

The 40 ms capture time corresponds to two full periods of the mains voltage signal, and is implemented to allow the ringing - caused by the filter's impulse response - to be truncated. After this process, the signals need to be rearranged to let the first data point ($t(0)$) correspond to T_0 ($\Theta_{\text{mains}} = 0°$). This method is also shown in Fig. 11 and Fig. 12.

The impedance Z, from (9) cannot be calculated continuously. As (9) shows, there is a division where the signals V_2 and I_2 are in the denominator. Both signals cross zero twice each period, causing a mathematical error where the impedance becomes undefined. Both the lack of dynamic range and the presence of noise in the measurement system causes the impedance to reach towards either $\pm$ infinity, as shown in Fig. 13.

A 'find-peak algorithm' has been implemented to resolve this issue. As Fig. 13 shows, the peaks of V_1 and V_2 give the timestamps where Z can be determined most accurately. The algorithm finds both positive and negative extrema of the V_2 signal and places a frequency-dependent number of indicators (within 5% signal's wavelength) near these extrema to account for the noise in the system, which is assumed to be white and Gaussian. The timestamps of these extrema are used to find the corresponding values of V_1. A more accurate representation of

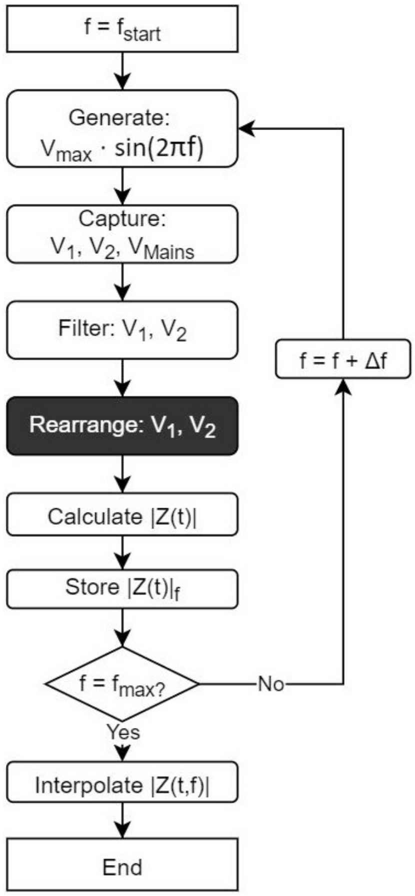

Fig. 10: Measurement algorithm

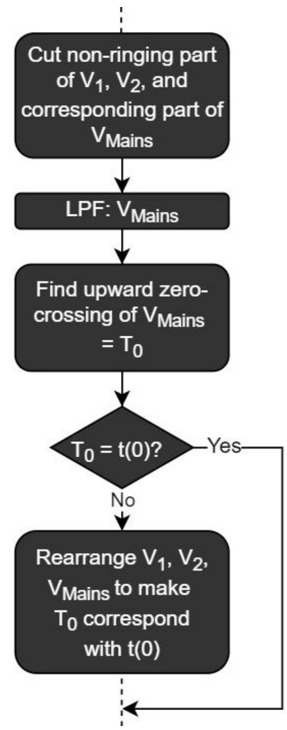

Fig. 11: Signal rearrangement algorithm

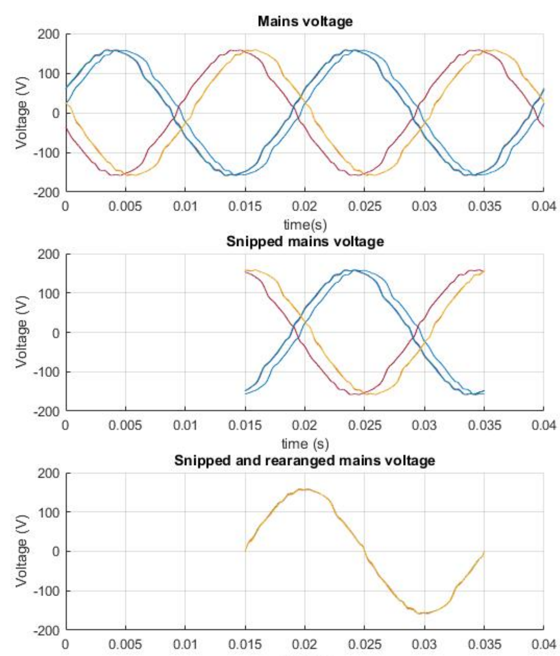

Fig. 12: Truncating and rearranging 10 mains voltage signals

(9) is thus given by:

$$Z = \frac{V_1(t_{pks}) - A_{inj} \cdot N - B_{inj} \cdot M}{A_{inj} \cdot M} \tag{10}$$

Where:

$$\begin{aligned} N &= V_2(t_{pks}) \cdot A_{rec} + I_2(t_{pks}) \cdot B_{rec} \\ M &= V_2(t_{pks}) \cdot C_{rec} + I_2(t_{pks}) \cdot D_{rec} \end{aligned} \tag{11}$$

The t_{pks} parameter represent the time instances surrounding the extrema of V_2.

While (7) provides a complex representation of the impedance, it is converted to its absolute form in order to accelerate the measurement and to prevent the DAQ from running out of memory. While information about the angle of the NUT's impedance can be useful, it is not often sought after and not required to validate the proposed measurement setup. It is therefore neglected here, and assumed to be as obtainable and legitimate as the $|Z|$ measurement.

A new signal of a higher frequency can be generated after the found $|Z|$ is stored until all frequencies of interest have been accounted for. The last step in this process covers an interpolation process which is required due to the find-peak algorithm. As the impedance is only calculated during the peaks of V_2, and the number of peaks is linearly dependent on the signal's frequency, the data array of the starting frequency will be shorter than that of the last frequency. The

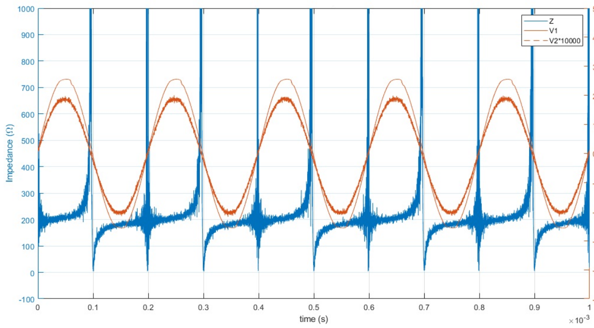

Fig. 13: Continuous calculation of a 200 Ω impedance

interpolation process adds data to all arrays smaller than the largest one in order to make them equally long.

V. Measurement results

While the measurement setup has been validated in section III-B, there are two complications that have not yet been accounted for.

A. Unreliability at high and low frequencies

Fig. 9i demonstrates a fairly accurate measurement of a 50 Ω resistive network, with maximum deviations of +2.8 Ω at 16 kHz and -2.5 Ω at 256 kHz. When the frequency range is expanded from 16 kHz - 256 kHz to 2 kHz - 1 MHz (Fig. 14), these deviations are shown to increase significantly.

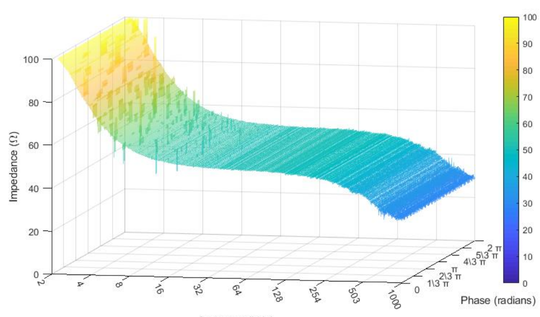

Fig. 14: Measurement setup becomes unreliable outside the proposed frequency range

Even though this problem has not yet been resolved, it is presumed to originate from the phase characteristics of the system, or more precisely, from characterization errors made while determining the probes' phases. When the setup validation shown in Fig. 9d and 9e is repeated for frequencies below 16 kHz and above 256 kHz (Fig. 15), it can be seen that (1a) does not hold anymore.

Comparing Fig. 14, 16 and 17 provides a means to theorize a potential origin of these errors. It was found that the setup showed lower inaccuracies in the lower frequency range

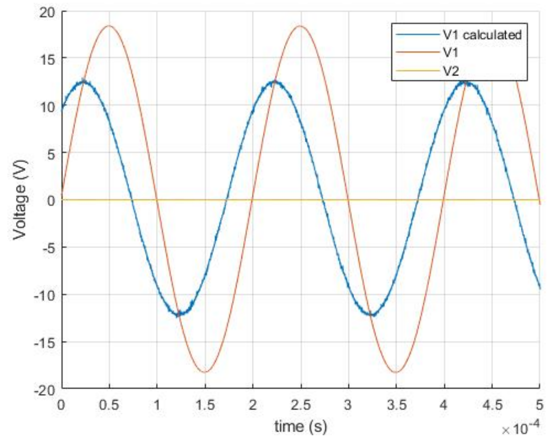

Fig. 15: Reproducing V_1 becomes erroneous outside proposed frequency (5 kHz signal)

where $f < 40$ kHz when no HPF is implemented in the system. The setup functions comparably at $f > 40$ kHz. Fig. 16 shows little justification to assume a lack of dynamic range to be the source of these errors, as the setup's magnitude does not vary between 16 kHz and 256 kHz, while the measured impedance certainly does. Fig. 16 does however give reason to consider either a high $\frac{d\theta}{df}$ or just phase shifts in general to be a possible causation.

Reiterating the validation process based on (1a) showed results conforming with this hypothesis. Where the receiving probe was significantly worse than the injecting probe at frequencies below 10 kHz, but comparable at frequencies above 100 kHz. Comparing these findings with Fig. 7 explains the reasoning behind these hypotheses. Given the magnitude of the receiving probe's S_{21} parameter, it would be expected to operate better than the injecting probe for all frequencies above 300 Hz. If it are the probes' angle characteristics however, that are causing these errors, it can be understood why the receiving probe is worse at frequencies below 40 kHz, and comparable at frequencies above 100 kHz.

Recognizing that (7) provides the NUT's impedance based on the difference between the input- and output signal makes it clear why errors in the phase characterization have such a significant impact on the impedance measurement. Comparing the output signal to the input signal at different angles will necessarily result in incorrect measurements. A similar principle also applies to the validation process. Due to the $[Mag + Phase] \rightarrow [Re + Im]$ conversion, a faulty phase characterization will result in both phase- and magnitude errors (Fig. 15).

The find-peak algorithm gives reason to expect the accuracy to increase when the phase shift approaches zero i.e. when the peaks of V_1 and V_2 align. That is, at an angle close to 90

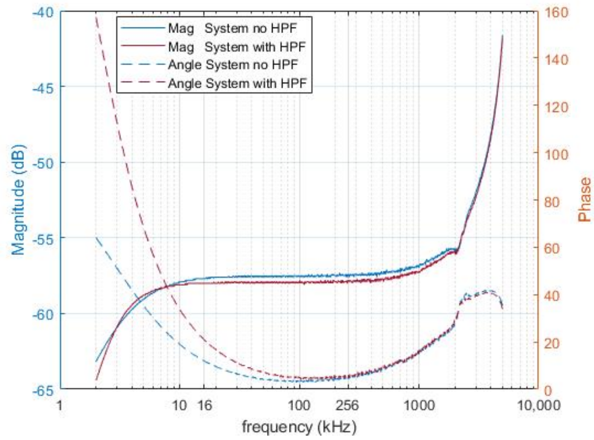

Fig. 16: Setup characterization, with and without HPF

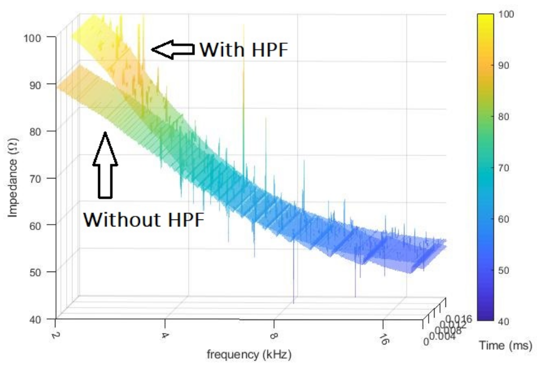

Fig. 17: Comparison of a $50\,\Omega$ measurement by a setup with- and without an HPF

degrees the peak of V_2 will be compared to the zero crossing of V_1, where noise is most dominant. A quick comparison of Fig. 14 with Fig. 16 refutes the latter hypotheses however, as an angle of 160 degrees at 2 kHz should provide a more accurate measurement than the 90 degree angle at roughly 4 kHz. This insight also opposes the instinctive thought that these errors are chiefly caused by a low signal-to-noise ratio (SNR).

B. Complex impedance

While the translation of the network from Fig. 3 into its transmission parameters as given in [11] and shown in (5) was validated for resistive loads, it appears to be invalid for non-resistive loads. A complex impedance forces a phaseshift in the current drawn by the respective load. Hence, calculating the impedance with (12) results in a meaningless value where the sinusoidal functions are not erased by the division, causing the 'impedance' to behave like a tangent function.

$$B_{Mains} = \frac{V(t)}{I(t)} = \frac{V_{\max} sin(\omega\ t)}{I_{\max} sin(w\ t + \phi)} \neq Z \tag{12}$$

An accurate formula to retrieve a complex impedance, which is still considerably applicable for the proposed setup is given in [12]:

$$Z = \frac{V_{\max}}{I_{\max}} \cdot e^{j \cdot \phi} \tag{13}$$

Where ϕ denotes the phase difference between the voltage and current of the respective load. The exponent provides an imaginary factor to the impedance, and gives information about its phase shift. It disappears when the absolute impedance is calculated, due to $|x \cdot y| = |x| \cdot |y|$ and $|e^{j \cdot x}| = 1$.

Substituting the $\mathrm{V_{LE}}$ probe for a V_{LN} probe allows to find the voltage V_{Mains} from the B_{mains} parameter shown in (5). The corresponding current can be determined by $\frac{V_{\mathrm{Mains}}}{B_{\mathrm{Mains}}}$, whereafter $V_{\max}$, $I_{\max}$ and $|Z|$ from (13) can be found.

C. Mains impedance measurement

As the measurement errors described in sections V-A and V-B have not been resolved yet, it is to no surprise that an actual mains impedance measurement is riddled with errors. A logical first measurement would be to measure the impedance of a live Line Impedance Stabilization Network (LISN), where a stable $50\,\Omega$ impedance would be the expected result. But due to a combination of external obstacles and a faulty measurement, this had to be left out of this paper.

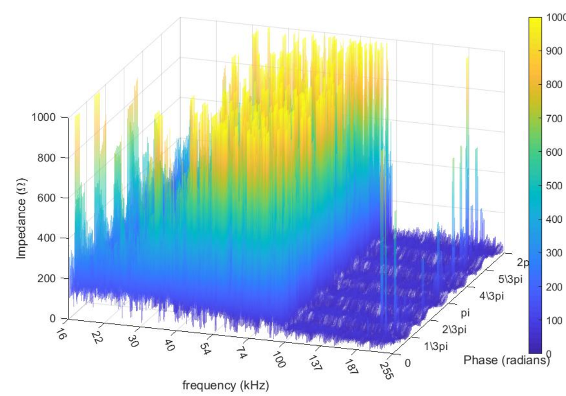

Fig. 18: Mains impedance measurement (16 kHz - 256 kHz)

An actual mains impedance measurement is shown in Fig. 18. The flawed nature of this measurement makes it nearly impossible to retrieve any useful information from it. Especially the measurements in the 40 kHz - 100 kHz frequency band seem very inaccurate, but whether this is caused by non-resistive mains impedances, harmonic signals, a lack of dynamic range, or something different is unknown. Fig. 20 does imply the dynamic range of the system to be insufficient i.e. to be at least partly responsible for the misreadings, as the signals magnitude is considerably lower than the harmonics of the 50 Hz mains voltage. At a measurement signal of 143 kHz (Fig. 21), this problem seems to be less prominent, presumably due to a lower mains impedance.

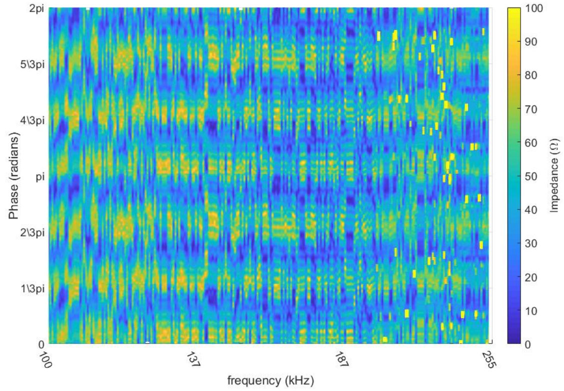

Fig. 19: Mains impedance measurement (100 kHz - 256 kHz)

While the impedance plane between 100 kHz and 256 kHz seems to be free of errors, it shows impedances far above what is to be expected (Fig. 19). At 255 kHz the absolute impedance varies between 8 Ω and 72 Ω, while [1] shows an impedance of less than 1 Ω at this frequency. It should simultaneously be recognized that the mains impedance can vary drastically between different locations and networks [8], so it's not necessarily an inaccurate measurement. Ultimately, little can be said about the validity of this measurement as long as measurements of known live network impedances are unobtainable.

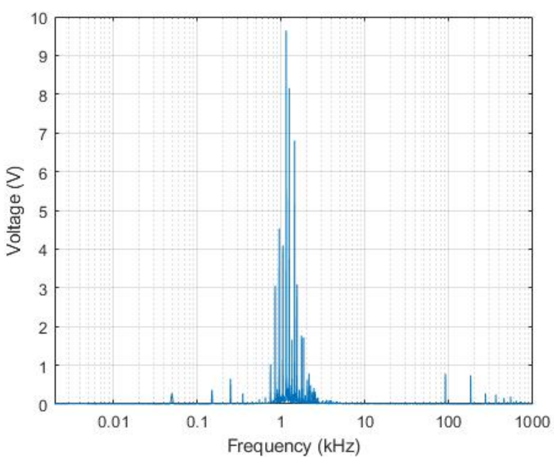

Fig. 20: FFT of V_2 at f_{signal} = 91 kHz

VI. Conclusion

A non-intrusive impedance measurement setup has been designed, it determines network impedances in both time- and frequency domain (16 kHz - 256 kHz). The setup injects and records signals into the NUT by means of specifically designed current transformers, the NUT's impedance is then calculated based on the probes' transmission paramters. While the setup still lacks accuracy due to insufficient dynamic range and errors caused by angles between the injected current and the subsequent voltage within the NUT, it still holds promise as these problems are surmountable. The introduced algorithm can also be implemented in similar setups such as [7], to enhance them with the ability to measure time-variant impedances.

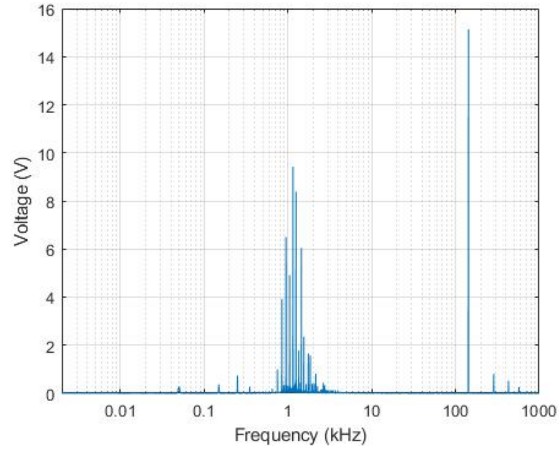

Fig. 21: FFT of V_2 at f_{signal} = 143 kHz

VII. Recommendations

As stated previously, the constructed measurement setup requires improvements in order to actually measure mains impedances. The most substantial upgrade would involve the amplifier, as roughly two thirds of the measurements are executed by an audio amplifier that regularly overheats and generates an unpredictable amount of harmonic distortion that significantly affects the measurement's accuracy. Further recommendations are listed here.

A. Dynamic range

In addition to enhancing the amplification, the dynamic range can be increased with improved current transformers. Space was the main limitation in the design of the injection probe due to the already large size of the receiving probe and the fact that they both needed to fit inside the calibration fixture. The receiving probe can be re-designed to decrease its size, as this was not an initial concern. Building a calibration fixture for these specific transformers is simultaneously a solution this problem.

B. Load impedance

In addition to enhancing the amplification, the dynamic range can be increased by complementing the resistive 100 Ω load impedance Z_{Load} with a capacitor C_{Load} to block the 50 Hz mains current. The value of C_{Load} should be chosen such that its impedance becomes negligibly small at the starting frequency i.e. that it does not influence either the phase or the magnitude of the excitation signal. The characterization process of Section II-B2 does not need revision if this requirement is met.

C. Filter design

A 1 kHz analog HPF was implemented in the measurement setup to filter the 50 Hz mains signal without conceding in dynamic range. While this approach functions as a means to filter the mains voltage, it brings a new limitation in the system's ability to measure time-variant impedances. Since these impedances are shown as fluctuations in V_2's amplitude, the HPF will filter any slow varying impedances. The ideal solution would be a sharp 50 Hz notch filter with little ringing. Concessions can be made in its phase characteristics as these can be neglected outside the frequency band of interest. Where it is important to realize that the signal's frequency is distinct from the impedance's frequency.

D. Measurement accuracy

The measurement setup, in its current state, does not have a sufficient precision to accurately determine impedances within low ohmic regions. Especially at frequencies below 10 kHz the mains impedance is very low, descending to values below $0.1\,\Omega$ [8]. In other setups such as [9] and [13] linear power amplifiers with an output current of 10 A and an output power 2.2 kW are used. The measurements conducted for this paper depended on a 100 W audio amplifier for $f_{\text{signal}} \leq 100\,\text{kHz}$ and a 10 W RF amplifier for $f_{\text{signal}} > 100\,\text{kHz}$. Recognizing that the signal is injected into the NUT via a current transformer, makes it evident that both current- and power amplifiers are more suitable than the voltage amplifier used in the lower frequency region of this measurement setup. It is furthermore expected that the setups accuracy is primarily dependent on its SNR, therewith the amplifiers gain.

E. Unreliability outside proposed frequency band

Section V-A described the phenomenon displayed in Fig. 14, where the setups reliability decreases as its S-21 angle increases. While the exact cause has yet to be found, a workaround can still be devised. A somewhat tricky approach would be to determine the probes' transmission parameters solely on the magnitude of their S-parameters. The S-21 phase information can be used in the data acquisition to revert the shifts caused by the current transformers. Hereafter, the angle between V_1 and V_2 is solely provided by the NUT.

References

[1] M. Coenen and A. v. Roermund, "'Live' Mains Impedance Measurement and Analysis ," *S International Symposium on Electromagnetic Compatibility*, 2013.

[2] M. Bridgeman, R. Morrison, and S. Tenakoon, "Measurement of harmonic impedance on an LV system utilising power capacitor switching and consequent predictions of capacitor induced harmonic distortion," 1998.

[3] *International Electrotechnical Commission–CISPR 22–Amendment 1–Information technology equipement - Radio disturbance characteristics - Limits and methods of measurement*, 2001.

[4] L. B. Wang, P. L. So, K. Y. See, M. Oswal, and T. S. Pang, "Investigation of Radiated Emissions in Power Line Communications Networks," *International Journal of Emerging Electric Power Systems*, vol. 9:3, 2008.

[5] B. Have, T. Hartman, N. Moonen, C. Keyer, and F. Leferink, "Faulty Readings of Static Energy Meters Caused by Conducted Electromagnetic Interference from a Water Pump," *Renewable Energy and Power Quality Journal*, 2019.

[6] S. B. Rathnayaka, K.-Y. See, and K. Li, "On-line Impedance Monotoring of Transformer Based on Inductive Coupling Approach," *IEEE Transactions on Dielectrics and Electrical Insulation*, 2017.

[7] J. Tan, "In-situ impedances measurement and influence of 2 k - 150 kHz disturbances on measurement of electrical parameters," Master's thesis, Delft University of Technology, 2019.

[8] R. Stiegler, J. Meyer, S. Schori, M. Höckel, and K. Scheida, "SURVEY OF NETWORK IMPEDANCE IN THE FREQUENCY RANGE 2-9 KHZ IN PUBLIC LOW VOLTAGE NETWORKS IN AT/CH/CZ/GE," *25th International Conference on Electricity Distribution*, 2019.

[9] R. Stiegler, J. Meyer, P. Schegner, and D. Chakravorty, "Measurement of network harmonic impedance in presence of electronic equipment," 2015.

[10] Z. Zhao, K.-Y. See, E.-K. Chua, A. S. Narayanan, W. Chen, and A. Weerasinghe, "Time-Variant In-Circuit Impedance Monitoring Based on the Inductive Coupling Method," *IEEE Transactions on Instrumentation and Measurement*, 2019.

[11] D. M. Pozar, *Microwave Engineering, 4th Edition*. Wiley, 2012.

[12] T. Jacobson, "Complex impedance method for AC circuits," *Supplement — Phy273*, 2002.

[13] D. Chakravorty, J. Meyer, P. Schegner, S. Yanchenko, and M. Schocke, "Impact of Modern Electronic Equipment on the Assessment of Network Harmonic Impedance," *IEEE Transactions on Smart Grid*, 2017.